

Reconfigurable microfluidic photonic crystal slab cavities

Cameron L. C. Smith,^{1,*} Uwe Bog,¹ Snjezana Tomljenovic-Hanic,¹ Michael W. Lee,¹ Darran K. C. Wu,¹ Liam O'Faolain,² Christelle Monat,¹ Christian Grillet,¹ Thomas F. Krauss,² Christian Karnutsch,¹ Ross C. McPhedran,¹ Benjamin J. Eggleton¹

¹Centre for Ultrahigh-bandwidth Devices for Optical Systems (CUDOS), School of Physics
University of Sydney, Sydney, NSW 2006, Australia

²School of Physics and Astronomy, University of St. Andrews, St. Andrews, Fife KY16 9SS, Scotland

*Corresponding author: c.smith@physics.usyd.edu.au

Abstract: We demonstrate the spectral and spatial reconfigurability of photonic crystal double-heterostructure cavities in silicon by microfluidic infiltration of selected air holes. The lengths of the microfluidic cavities are changed by adjusting the region of infiltrated holes in steps of several microns. We systematically investigate the spectral signature of these cavities, showing high Q -factor resonances for a broad range of cavity lengths. The fluid can be removed by immersing the device in toluene, offering complete reconfigurability. Our cavity writing technique allows for tolerances in the infiltration process and provides flexibility as it can be employed at any time after photonic crystal fabrication.

©2008 Optical Society of America

OCIS codes: (230.5298) Photonic crystals; (280.4788) Optical sensing and sensors.

References and links

1. D. Psaltis, S. R. Quake, and C. H. Yang, "Developing optofluidic technology through the fusion of microfluidics and optics," *Nature* **442**, 381-386 (2006).
2. C. Monat, P. Domachuk, and B. J. Eggleton, "Integrated optofluidics: A new river of light," *Nat. Photon.* **1**, 106-114 (2007).
3. M. Loncar, A. Scherer, and Y. M. Qiu, "Photonic crystal laser sources for chemical detection," *Appl. Phys. Lett.* **82**, 4648-4650 (2003).
4. M. L. Adams, M. Loncar, A. Scherer, and Y. M. Qiu, "Microfluidic integration of porous photonic crystal nanolasers for chemical sensing," *IEEE J. Sel. Areas Commun.* **23**, 1348-1354 (2005).
5. S. Balslev, A. M. Jorgensen, B. Bilenberg, K. B. Mogensen, D. Snakenborg, O. Geschke, J. P. Kutter, and A. Kristensen, "Lab-on-a-chip with integrated optical transducers," *Lab on a Chip* **6**, 213-217 (2006).
6. S. S. Xiao, and N. A. Mortensen, "Proposal of highly sensitive optofluidic sensors based on dispersive photonic crystal waveguides," *J. Opt. A: Pure Appl. Opt.* **9**, S463-S467 (2007).
7. S. H. Kim, J. H. Choi, S. K. Lee, S. H. Kim, S. M. Yang, Y. H. Lee, C. Seassal, P. Regreny, and P. Viktorovitch, "Optofluidic integration of a photonic crystal nanolaser," *Opt. Express* **16**, 6515-6527 (2008).
8. K. Busch and S. John, "Liquid-crystal photonic-band-gap materials: The tunable electromagnetic vacuum," *Phys. Rev. Lett.* **83**, 967-970 (1999).
9. P. Mach, M. Dolinski, K. W. Baldwin, J. A. Rogers, C. Kerbage, R. S. Windeler, and B. J. Eggleton, "Tunable microfluidic optical fiber," *Appl. Phys. Lett.* **80**, 4294-4296 (2002).
10. B. Maune, M. Loncar, J. Witzens, M. Hochberg, T. Baehr-Jones, D. Psaltis, A. Scherer, and Y. M. Qiu, "Liquid-crystal electric tuning of a photonic crystal laser," *Appl. Phys. Lett.* **85**, 360-362 (2004).
11. J. C. Galas, J. Torres, M. Belotti, Q. Kou, and Y. Chen, "Microfluidic tunable dye laser with integrated mixer and ring resonator," *Appl. Phys. Lett.* **86**, 264101 (2005).
12. D. Erickson, T. Rockwood, T. Emery, A. Scherer, and D. Psaltis, "Nanofluidic tuning of photonic crystal circuits," *Opt. Lett.* **31**, 59-61 (2006).
13. F. B. Arango, M. B. Christiansen, M. Gersborg-Hansen, and A. Kristensen, "Optofluidic tuning of photonic crystal band edge lasers," *Appl. Phys. Lett.* **91**, 223503 (2007).
14. A. Groisman, S. Zamek, K. Campbell, L. Pang, U. Levy, and Y. Fainman, "Optofluidic 1x4 switch," *Opt. Express* **16**, 13499-13508 (2008).
15. P. El-Kallassi, S. Balog, R. Houdre, L. Balet, L. Li, M. Francardi, A. Gerardino, A. Fiore, R. Ferrini, and L. Zuppiroli, "Local infiltration of planar photonic crystals with UV-curable polymers," *J. Opt. Soc. Am. B* **25**, 1562-1567 (2008).

16. E. Chow, A. Grot, L. W. Mirkarimi, M. Sigalas, and G. Girolami, "Ultracompact biochemical sensor built with two-dimensional photonic crystal microcavity," *Opt. Lett.* **29**, 1093-1095 (2004).
17. S. Kita, K. Nozaki, and T. Baba, "Refractive index sensing utilizing a cw photonic crystal nanolaser and its array configuration," *Opt. Express* **16**, 8174-8180 (2008).
18. T. F. Krauss, "Photonic crystals - Cavities without leaks," *Nat. Mater.* **2**, 777-778 (2003).
19. K. J. Vahala, "Optical microcavities," *Nature* **424**, 839-846 (2003).
20. B. S. Song, S. Noda, and T. Asano, "Photonic devices based on in-plane hetero photonic crystals," *Science* **300**, 1537-1537 (2003).
21. E. Centeno, and D. Felbacq, "Optical bistability in finite-size nonlinear bidimensional photonic crystals doped by a microcavity," *Phys. Rev. B* **62**, R7683-R7686 (2000).
22. B. S. Song, S. Noda, T. Asano, and Y. Akahane, "Ultra-high-Q photonic double-heterostructure nanocavity," *Nat. Mater.* **4**, 207-210 (2005).
23. C. L. C. Smith, D. K. C. Wu, M. W. Lee, C. Monat, S. Tomljenovic-Hanic, C. Grillet, B. J. Eggleton, D. Freeman, Y. Ruan, S. Madden, B. Luther-Davies, H. Giessen, and Y. H. Lee, "Microfluidic photonic crystal double heterostructures," *Appl. Phys. Lett.* **91**, 121103 (2007).
24. F. Intonti, S. Vignolini, V. Turck, M. Colocci, P. Bettotti, L. Pavesi, S. L. Schweizer, R. Wehrspohn, and D. Wiersma, "Rewritable photonic circuits," *Appl. Phys. Lett.* **89**, 211117 (2006).
25. S. Tomljenovic-Hanic, C. M. de Sterke, and M. J. Steel, "Design of high-Q cavities in photonic crystal slab heterostructures by air-holes infiltration," *Opt. Express* **14**, 12451-12456 (2006).
26. J. Li, T. P. White, L. O'Faolain, A. Gomez-Iglesias, and T. F. Krauss, "Systematic design of flat band slow light in photonic crystal waveguides," *Opt. Express* **16**, 6227-6232 (2008).
27. "Datasheet TYPIOB, Immersion Oil Type B," (Cargille Laboratories, 2002).
28. J. C. Knight, G. Cheung, F. Jacques, and T. A. Birks, "Phase-matched excitation of whispering-gallery-mode resonances by a fiber taper," *Opt. Lett.* **22**, 1129-1131 (1997).
29. P. E. Barclay, K. Srinivasan, M. Borselli, and O. Painter, "Probing the dispersive and spatial properties of photonic crystal waveguides via highly efficient coupling from fiber tapers," *Appl. Phys. Lett.* **85**, 4-6 (2004).
30. C. Grillet, C. Smith, D. Freeman, S. Madden, B. Luther-Davis, E. C. Mägi, D. J. Moss, and B. J. Eggleton, "Efficient coupling to chalcogenide glass photonic crystal waveguides via silica optical fiber nanowires," *Opt. Express* **14**, 1070-1078 (2006).
31. I. K. Hwang, S. K. Kim, J. K. Yang, S. H. Kim, S. H. Lee, and Y. H. Lee, "Curved-microfiber photon coupling for photonic crystal light emitter," *Appl. Phys. Lett.* **87**, 131107 (2005).
32. X. Letartre, C. Seassal, C. Grillet, P. Rojo-Romeo, P. Viktorovitch, M. L. d'Yerville, D. Cassagne, and C. Jouanin, "Group velocity and propagation losses measurement in a single-line photonic-crystal waveguide on InP membranes," *Appl. Phys. Lett.* **79**, 2312-2314 (2001).
33. M. Notomi, K. Yamada, A. Shinya, J. Takahashi, C. Takahashi, and I. Yokohama, "Extremely large group-velocity dispersion of line-defect waveguides in photonic crystal slabs," *Phys. Rev. Lett.* **87**, 253902 (2001).
34. K. Srinivasan and O. Painter, "Fourier space design of high-Q cavities in standard and compressed hexagonal lattice photonic crystals," *Opt. Express* **11**, 579-593 (2003).
35. U. Bog, C. L. C. Smith, M. W. Lee, S. Tomljenovic-Hanic, C. Grillet, C. Monat, L. O'Faolain, C. Karnutsch, T. F. Krauss, R. McPhedran, and B. J. Eggleton, "High-Q microfluidic cavities in silicon-based 2D photonic crystal structures," *Opt. Lett.* **33** (2008).
36. C. Schuller, F. Klopff, J. P. Reithmaier, M. Kamp, and A. Forchel, "Tunable photonic crystals fabricated in III-V semiconductor slab waveguides using infiltrated liquid crystals," *Appl. Phys. Lett.* **82**, 2767-2769 (2003).

1. Introduction

Optofluidics is an emerging field of research that integrates microfluidics with nano-photonics. Demonstrations of optofluidic devices exploit the characteristics of fluids to achieve dynamic manipulation of optical properties and reveal the promise for their widespread use [1, 2]. There is, on the one hand, a potential to realize highly sensitive integrated sensors [3-7], while on the other, a flexible means to write, tune or reconfigure photonic devices for a swathe of applications [8-15]. Recently there have been advances in the development of fully integrated microfluidic and photonic platforms [11-13]. In this regard, it has been shown that photonic crystals (PhCs) in general [6, 9, 12, 13] and PhC cavities in particular [3, 7, 10, 15-17] can be advantageously exploited within optofluidic architectures. The latter is due to the potentially high light-liquid interaction that occurs when infiltrating the air holes that typically surround and/or form the PhC cavity.

PhC cavities have received much interest in recent years due to their ability to strongly confine light on the wavelength scale [18, 19]. This capability promotes their use in numerous applications, including channel-drop filters [20] and optical switching [21]. PhC cavities are

created by altering the periodicity of the PhC through the introduction of a defect (such as removal or positional shift of air holes). Song *et al.* demonstrated more recently “double-heterostructure” (DH) PhC cavities [22], where two PhC geometries containing slightly different lattice parameters are combined. This is done in such a way that light is spatially confined within the central section of the PhC where the effective refractive index is larger. However, all these approaches present certain drawbacks when combining the generated PhC cavity with microfluids. First, this requires precise alignment between the micro-scale defect forming the PhC cavity and the liquid to be infiltrated; or alternatively demands a large amount of liquid which is not practical in many sensing applications. Second, the properties of PhC cavities are static when geometry-based, lacking flexibility. Lastly, the Q -factor of the geometry-based PhC cavity is typically degraded after the infiltration step [3], which is detrimental to the performance in both the sensing and optical device regimes.

By contrast, we demonstrate an approach for realizing optofluidic PhC cavities, based on a principle similar to the DH but able to overcome most of the difficulties mentioned above. The technique relies on the selective infiltration of a section of an otherwise cavity-free PhC structure [23, 24]. First, the optofluidic PhC cavities are created during the infiltration step, relaxing the constraint on alignment between the fluid and a pre-existing micro-scale cavity. Second, these cavities can be configured in a flexible manner by altering the size or geometry of the infiltrated region as well as the refractive index of the liquid. The optofluidic structures may then be reconfigured by removing the fluid and returning the PhC to its original state. Third, these cavities exhibit high Q -factors despite the presence of a fluid: it has been shown that this microfluidic regime may potentially reach Q -factors of $Q = 1 \times 10^6$ [25].

In this paper we demonstrate the spectral and spatial reconfigurability of such optofluidic PhC DH cavities made in silicon by controlling the size of the selectively infiltrated region of air holes with fluid using a glass micro-tip. The microfluidic PhC cavity dimensions are altered by infiltrating a greater region of the holes to micrometer accuracies. The spectral signature measured from the generated microfluidic cavities is in good agreement with numerical simulations. Furthermore, we show that the Q -factor remains relatively high over a wide range of the cavity length, allowing for tolerances in the infiltration process. Eventually, the fluid is removable by immersing the infiltrated PhC in a bath of toluene, showing that this approach is a versatile method to create postprocessed and reconfigurable microcavities. Reconfigurable microfluidic PhC devices may be optimized for a broad scope of micron-scale all-optical applications integrated on a single chip, including sensing architectures and arbitrarily defined post-processed PhC structures.

2. Device and experiment

Figure 1(a) summarizes the principle of the microfluidic DH geometry. The adjacent regions (regular PhC) contain a regular triangular PhC lattice of air holes $n_{holes} = 1$, while the central region (infiltrated PhC) contains the same triangular PhC lattice yet with holes possessing an increased refractive index $n_{holes} = 1.5$ due to the presence of a fluid. A waveguide across the DH gives different dispersion curves associated with the different PhC sections. This results in the waveguide modes within the two sections existing at different frequencies. As illustrated in Fig. 1(b), this causes a “mode gap”, where light coupled to the waveguide mode of the infiltrated PhC section with a frequency lying in this gap does not propagate in the surrounding unchanged regular PhC section. Instead, the light remains localized, decaying evanescently in the adjacent regions.

The PhC structures are made from silicon, having a refractive index $n_{Si} = 3.52$ at 1.4 μm wavelength. We use a triangular lattice which nominally consists of a period $a = 410$ nm, suspended slab of thickness $T = 220$ nm ($0.537a$), and hole radius $r = 140$ nm ($0.341a$). A defect waveguide is introduced into these structures by removing one row of holes along the Γ - K direction of the lattice as shown in Fig. 1(a). The structures are 34 periods (14 μm) across by 61 periods (25 μm) along. The fabrication steps are identical to those used to create the devices of [26].

The two PhC sections to either side of the defect waveguide are shifted closer together by 35 nm each to reduce the guide width to 0.9 times the width of a W1 waveguide, creating a so-called W0.9. This modification is done to increase the frequency range between the fundamental waveguide mode and the low-frequency edge of the PhC photonic bandgap (PBG) (Fig. 1(b) and (c)). The mode gap corresponding to the infiltrated W0.9 therefore does not overlap the PBG edge and allows for a broad selection of fluid indices to configure our devices, where an increase in refractive index of the fluid extends the mode-gap. It is noticed that evanescent coupling to the structure is improved by using W0.9 waveguides rather than W1.

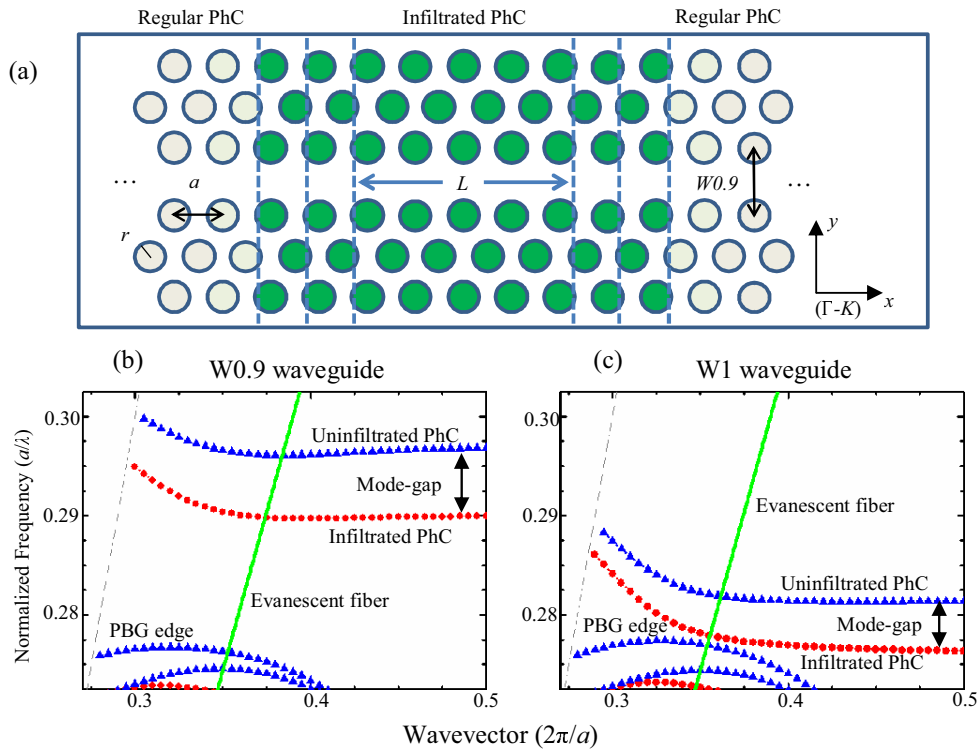


Fig. 1. (a) Schematic of fluid-filled PhC. (b) Calculated dispersion relation of the W0.9 PhC: blue triangles represent the PhC with air holes and red circles represent the PhC with fluid-filled holes. The green (solid) curve represents the evanescent coupling taper. The gray (dashed) curve represents the light-line. (c) Dispersion relation of a regular W1 waveguide with otherwise the same parameters as (b).

The fluid infiltration, illustrated in Fig. 2, is achieved by using a tapered glass micro-tip with apex diameter $\varnothing = 220$ nm. The micro-tip is controlled by a 3-axis piezo-electric stage (Thorlabs NanoMax) and is initially inserted within a meniscus of the filling fluid. We use a Cargille microscopy immersion oil type B of index $n_{fluid} = 1.50$ and absorption loss of 0.45 dB/cm at 1400 nm [27]. As the tip is withdrawn from the meniscus, droplets remain attached along its length due to adhesive forces between the glass and the fluid. These droplets are then deposited on the device chip beside the PhC structure under a microscope objective (Olympus BX61, LMPlanFl, 100 \times , 0.8 NA). This objective compromises between a large magnification to resolve properly the PhC waveguide and a sufficient working distance to allow for the micro-tip during infiltration. Lastly, the tapered glass micro-tip is used to draw a chosen droplet along the photonic crystal, perpendicular to the waveguide, to create the DH cavity.

The surface of the PhC and the particular fluid used each determine the penetration of the fluid into the pores of the PhC. If the fluid is phobic to the surface of the PhC, it forms a large meniscus and does not penetrate the air holes, instead remaining above. The selected immersion oil used in the experiments is philic to the surface. In this case, the fluid infiltrates the PhC holes via capillary action and remains suspended within them due to the fluid's surface tension. The selected fluid is also non-volatile and therefore does not evaporate out of the PhC pores.

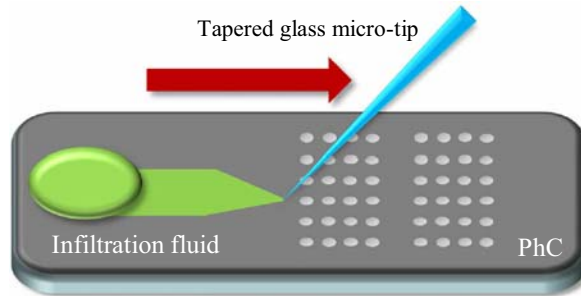


Fig. 2. Infiltration schematic: a glass micro-tip is used to draw the infiltration fluid across the PhC section, forming the DH stripe.

We investigate the fluid-filled DH cavities via evanescent coupling [28-30]. We use a standard single-mode fiber, reducing its diameter down from $125\ \mu\text{m}$ to $1.3\ \mu\text{m}$ over a length of 2 mm. Due to the reduction in diameter, the evanescent field of the propagating mode extends significantly beyond the tapered fiber's boundary, allowing it to interact with the PhC structure. Coupling can occur when there is a phase match between the fiber and PhC modes. Numerically, this is when dispersion curves of the taper and the PhC structure respectively intersect.

The tapered fibers have an intentionally induced shape to localize coupling to the micro-scale fluid-filled section of the DH. This is achieved by closing the fiber ends together after it had been tapered, twisting one end and then stretching the fiber ends apart. This forms a "loop" shape with a radius of approximately $30\ \mu\text{m}$. The looped nanowire is then annealed with a flame to "set" the silica glass and the induced shape. The loop is then pried open, leaving a "U" profile similar to [31].

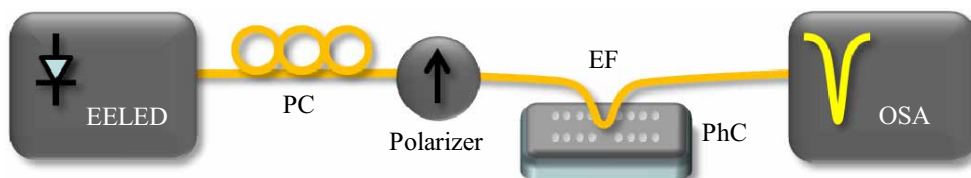


Fig. 3. Evanescent coupling schematic: polarization controller (PC) and polarizer select TE-like light from the edge-emitting light-emitting diode (EELED) source. The evanescent fiber (EF) couples light to the PhC sample and is connected to an optical spectrum analyzer (OSA) for monitoring.

The characterization setup is illustrated in Fig. 3. A broadband edge-emitting light-emitting diode source (HP 83437A) is connected to a polarization controller and polarizer that selects TE-like polarization (electric field lying in the plane of the PhC). The polarized light propagates through the nanowire, evanescently coupling to the PhC sample section and eventually monitored by an optical spectrum analyzer (OSA). Light coupled to the sample is not received at the OSA, resulting as a dip in the measured spectrum. A 6-axis nano-alignment system is utilized to position the nanowire and PhC sample. This process is imaged from above using a CCD camera and zooming lens.

3. Results

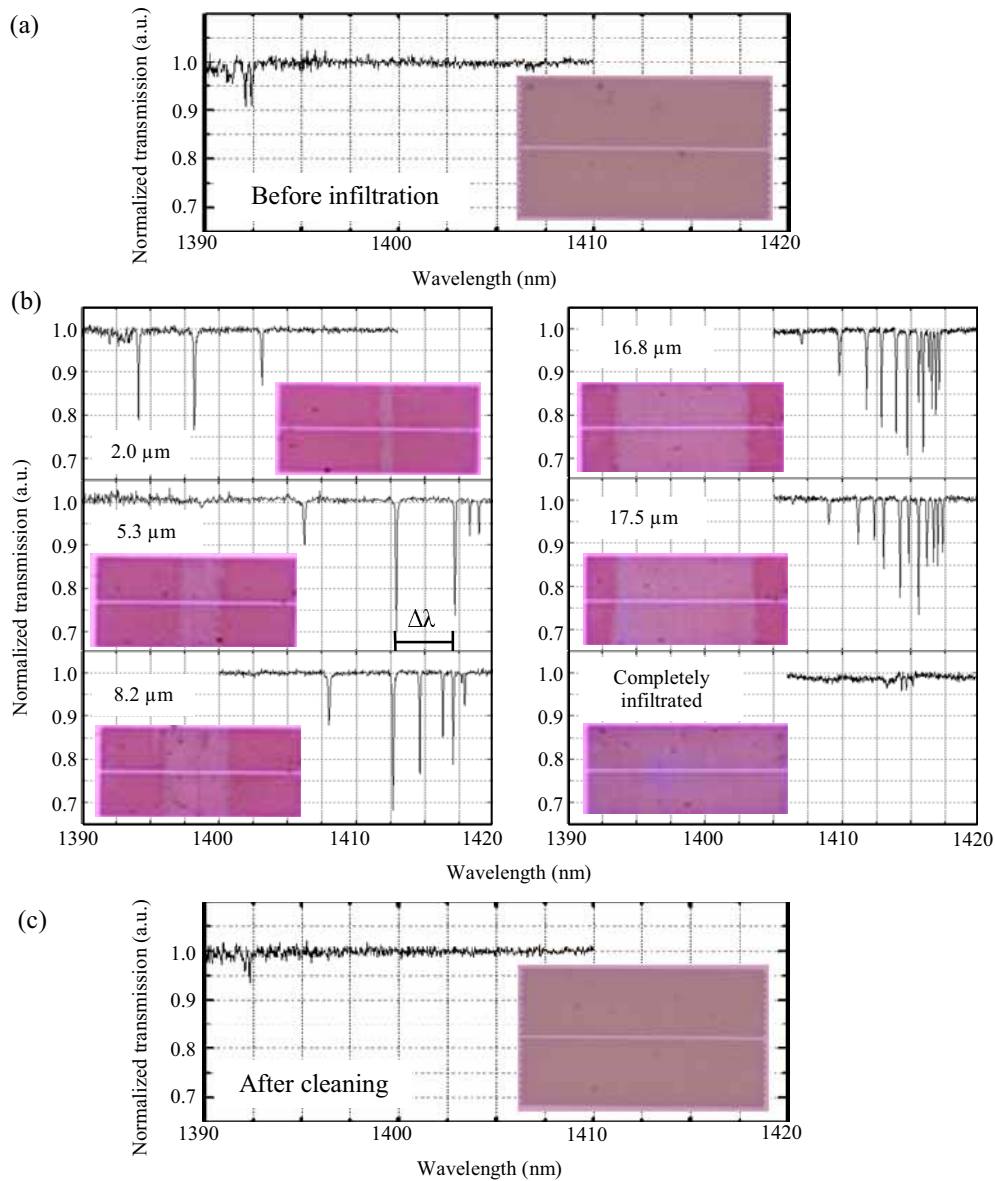


Fig. 4. (a) Spectrum of the case before infiltration. (b) Spectrum for varying infiltrated cavity lengths. (c) Spectrum of the case after cleaning. Insets are 150 \times microscope images of the corresponding waveguide/cavities.

The experiment starts with infiltrating a DH stripe (initially 2 μm) and incrementally increasing the infiltrated region on the same PhC structure in steps of ≈ 2 μm . Figure 4 shows the measurement spectra from the infiltration experiments. These correspond to the case before infiltration (Fig. 4(a)), the 2 μm , 5.3 μm , 8.2 μm , 16.8 μm and 17.5 μm length cavities plus completely infiltrated case (Fig. 4(b)) and the case after cleaning (Fig. 4(c)). Cleaning of the infiltrated PhC is achieved by immersing the sample in a bath of toluene for several minutes. We also write and characterize cavities of length 10.3 μm , 11.5 μm , 13.9 μm ,

20.1 μm and 21.3 μm , but for brevity are omitted. Each measured spectrum is obtained via evanescent coupling where the nanowire is out of contact with the structure. The cavities are imaged with a 150 \times , NA 0.9 microscope objective using a blue color filter to improve resolution. The resulting images are displayed in the insets of Fig. 4. For each, the contrast between the infiltrated and uninfiltrated PhC clearly attests the presence of the liquid into the middle of the structure, allowing us to estimate the respective width of the produced cavities.

The spectral signature of the initial PhC waveguide is measured before the infiltration process and shown in Fig. 4(a). The spectral dip at 1392 nm is associated with coupling to the fundamental TE-like waveguide mode. The discrete features are attributed to Fresnel reflections at the open ends of the PhC waveguide. After infiltration, (Fig. 4(b)), features appear at longer wavelengths. This is due to the increased effective refractive index of the modes from the presence of the fluid, as explained in Fig. 1. The observed fringe spectra are attributed to Fabry-Pérot (FP) modes sustained by the microfluidic cavity. The coupling strengths of the FP fringes with the taper are at a maximum where the phase-matching is strongest. It can be seen that as the cavity length increases, the fringe spacing becomes smaller, which is consistent with an increased density of modes for larger cavities. The wavelengths of the FP resonances should indeed closely meet the following condition:

$$2k_x L = 2\pi p, \quad (1)$$

which relates the wavevectors k_x of the FP resonances to the fluid-filled cavity length L through an integer p [32, 33]. When the PhC region is completely filled, the majority of these fringes disappear as the mode-gap effect no longer exists. In this case there is only coupling to the fluid-filled PhC fundamental waveguide mode, containing features that again occur due to Fresnel reflections at the open ends of the PhC structure. After fluid removal (Fig. 4(c)), the spectral signature is very similar to the case before infiltration.

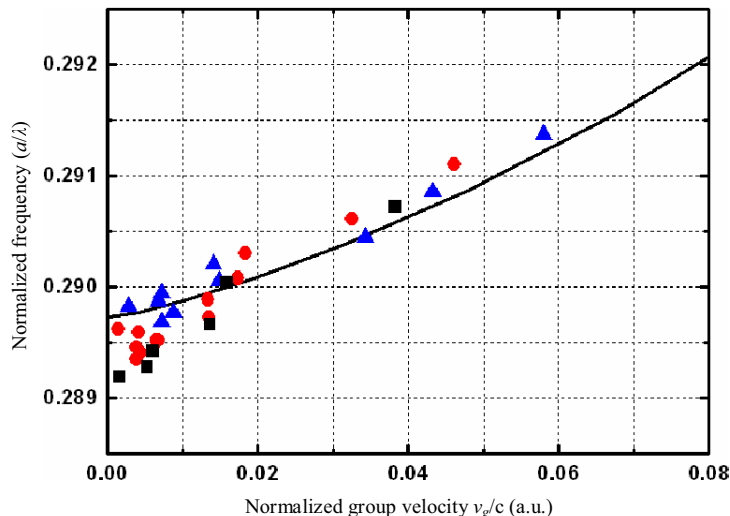


Fig. 5. Comparison of measured and calculated dispersive behavior for the fluid-filled PhCs. Cavity lengths of 8.2 μm (black squares), 16.8 μm (red circles) and 20.1 μm (blue triangles) are plotted against numerical data (black solid).

For each cavity length, the fringe spacing, $\Delta\lambda$, becomes smaller for increasing wavelength, which results from the dispersive nature of the PhC waveguide. The measured spectra are subsequently compared to the dispersion calculated for a W0.9 infiltrated waveguide using a three-dimensional plane-wave method with a supercell approach (RSoft's BandSOLVE) and the PhC parameters mentioned in Section 2. The result is shown in Fig. 5, which plots normalized frequency against group velocity and “maps” the dispersion. The calculated group velocity is

extracted from the gradient of the numerical dispersion relation, whereas the experimental group velocity is derived from the fringe spacing, $\Delta\lambda$, between the subsequent dips measured on the spectra of Fig. 4 and according to the equation $v_g = 2Lc\Delta\lambda/\lambda^2$. Note that the experimental dispersion curves derived for three different cavity lengths are reasonably superimposed, which is consistent with the fact that the FP modes all originate from the same dispersion relation, namely the one associated to the infiltrated W0.9 fundamental mode. In addition, this experimentally retrieved dispersion matches the calculated one within the bounds of fabrication tolerances.

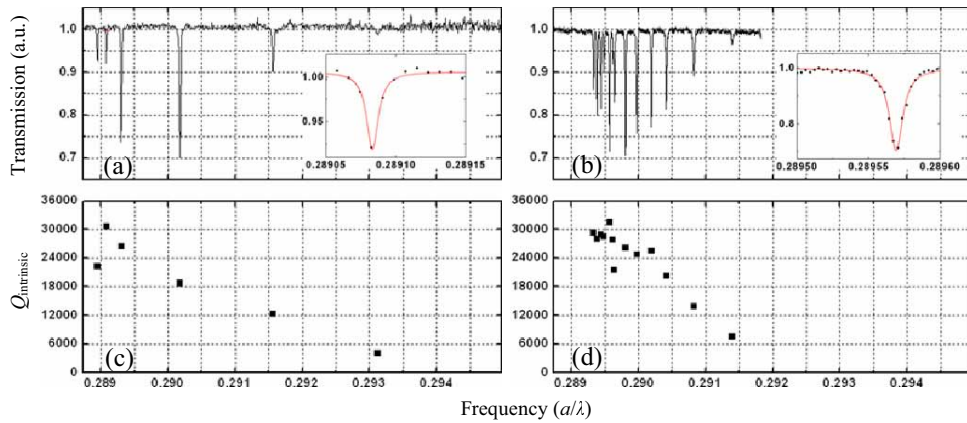


Fig. 6. Transmission and Q -factor versus frequency. (a) and (b) represent spectra from 5.3 μm and 16.8 μm cavity lengths with highest Q -factors shown inset. (c) and (d) are the corresponding Q -factors of the spectra to (a) and (b).

Next we consider the Q -factors associated to the modes of such optofluidic cavities. Figure 6 shows the trend of the mode Q -factor measured for two different cavity lengths (5.3 μm and 16.8 μm) as frequency increases. For each cavity, we have plotted their spectral signature (Fig. 6(a) and (b)) along with the corresponding Q -factors for each of the resonances revealed by the spectra (Fig. 6(c) and (d)). These two plots show the Q -factor increasing for a decreased frequency and this trend is representative of the whole set of cavity lengths. This is expected behavior [34], where the modes at lower frequency experience a higher effective index and thus better vertical confinement in the slab.

The Q -factors obtained in the experiments have values up to $Q = 3.5 \times 10^4$. The measurements are limited by the resolution of our OSA. More recent experiments have shown intrinsic Q -factors of $Q = 5.7 \times 10^4$ and these investigations will be reported elsewhere [35].

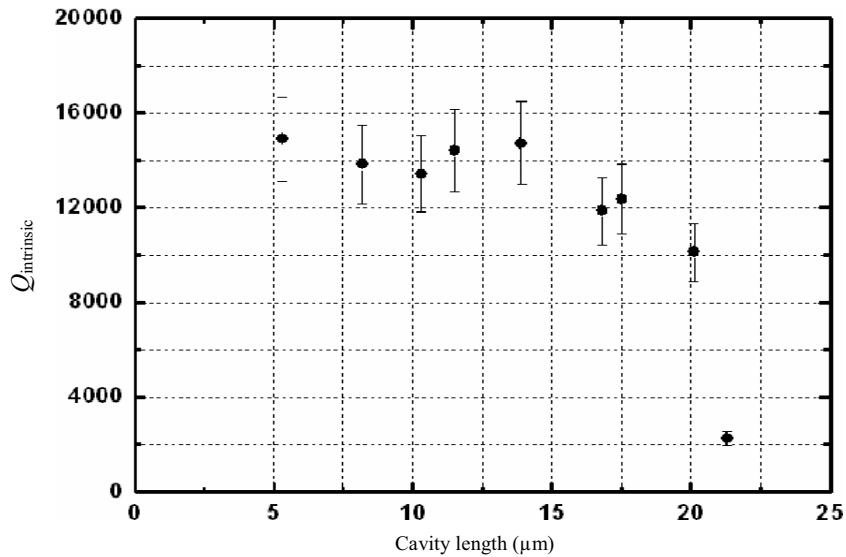


Fig. 7. Change of Q -factor against cavity length at an arbitrarily fixed frequency of $0.291 a/\lambda$. The entire PhC structure is $25 \mu\text{m}$.

We also investigate the Q -factor against cavity length at an arbitrarily fixed frequency of $0.291 a/\lambda$, which is high enough for avoiding resolution limited Q -factor values. This is shown in Fig. 7. We apply a linear fit to obtain the data as the spectral dips typically occurred to either side of this point. The $2 \mu\text{m}$ cavity length resonances occur away from this point, so is not included in this comparison. The Q -factor remains quite constant between $5.3 \mu\text{m}$ and $13.8 \mu\text{m}$. As the cavity lengths continue to increase from this point, the Q -factor drops as the in-plane confinement is reduced. This is due to the physically reduced unfiltered PhC section that provides the mode-gap. The trend continues through to the largest cavity length of $21.3 \mu\text{m}$ before the complete infiltration case. This suggests that $5 \mu\text{m}$ (12 holes in Γ - K direction) of unfiltered PhC section to each side of the microfluidic cavity is still large enough to maintain sufficient in-plane confinement. Note that the Q -factor remains larger than 10,000 for all cavity lengths excluding the $21.3 \mu\text{m}$ case, pointing out the large tolerances on the size of the infiltration region for generating reasonably high Q -factor modes with this approach.

4. Discussion

Our microfluidic approach to create flexible PhC cavities could feasibly be integrated within a chip-based microfluidic network in order to take full advantage of its reconfigurable characteristics. In this regard, there have been demonstrations of combining PhCs with microfluidics using a nanofluidic channel network to selectively address the intended PhC region [4, 7, 12]. These realizations rely on the challenging alignment between the PhC (linear or point) defect and the microfluidic delivery channel. By contrast, our approach is self-aligned: the structure forms *as a result* of the presence of fluid in the pores, which should make it less constraining to integrate within a microfluidic network. As opposed to the external method presented here that currently requires timescales on the order of minutes to reconfigure the device, a wholly integrated optofluidic platform should allow reconfigurable operation within seconds or milliseconds, as demonstrated in [12].

Liquid crystals (LCs) have been suggested in the past as a method to tune the static properties of PhC components [8]. LCs offer an index tuning range of $\Delta n \approx 0.05$ as achievable through electrical [10] or thermal [36] effects. This represents an order of magnitude less than what the available range of infiltration fluids could span: $n \approx 1.3 - 1.8$ ($\Delta n \approx 0.5$). Note that

because LCs offer a base index range of $n \approx 1.45 - 1.7$, they could be advantageously combined with our microfluidic double heterostructure scheme to provide both highly tunable (via electrical or thermal excitation) and reconfigurable (via fluid replacement) optical functionality.

5. Conclusion

We have reported a comprehensive study of microfluidic PhC DH cavities in silicon through the systematic comparison of the spectral properties of various cavity sizes created by this unique approach and supported by numerical simulations. Silicon is demonstrated to be well-suited to this approach. We have shown the spectral and spatial reconfigurability of the microfluidic cavities via flexible infiltration of selected holes. This technique offers a versatile solution for overcoming the many difficulties associated with integrating microfluidics with PhC cavities for sensing applications or tunable photonics. First, this approach is self-aligned in the sense that the optofluidic PhC cavities are created during the infiltration step, relaxing the constraint on alignment between the fluid and a pre-existing micro-scale cavity. Second, we have demonstrated that these cavities can be reconfigured in a flexible manner through control of the infiltrated region size combined with the possibility to “erase” the cavity by fully removing the fluid in toluene. Third, these cavities exhibit high Q -factors, which are here resolution limited, and this is achieved *because* of the presence of a fluid, rather than being degraded by it. Lastly, we show that the Q -factor of the generated modes remains high ($\approx 10,000$) over a large range of cavity lengths: 5 μm to 14 μm . In comparison with geometry perturbation schemes where precision is required to be nanometers, our approach extends this tolerance to the order of microns.

Acknowledgment

The support of the Australian Research Council through its Federation Fellow, Centre of Excellence and Discovery Grant programs is gratefully acknowledged. Additional acknowledgement is given to the support of the School of Physics, University of Sydney, through its Denison Foundation and the International Science Linkages program of the Department of Education, Science and Technology. The silicon samples were fabricated in the framework of the EU-FP6 funded ePIXnet Nanostructuring Platform for Photonic Integration (www.nanophotonics.eu).